II. ELECTRON MAGNETIC RESONANCE*

Academic Research Staff

Prof. K. W. Bowers

Graduate Students

Nancy H. Kolodny
C. Mazza
A. C. Nelson
L. S. Pensak
R. S. Sheinson
N. S. Suchard
Y.-M. Wong
B. S. Yamanashi

A. EXCITED STATES OF CARBONYL HYDROCARBONS

Electric dipole transitions in carbonyl hydrocarbons, in general, are more strongly polarized than in purely aromatic hydrocarbons.[1] The conventional empirical characterization of the orbital excitation identifies the phosphorescent state of benzophenone-like systems as $^3\Gamma_{n\pi^*}$.

The EMR measurements of $^3\Gamma_{n\pi^*}$ of benzophenone have been considered to be extremely difficult, because of the short lifetime $\tau_p \sim 10^{-3}$ sec, and hence a low steady-state concentration results.[2] Recently, however, the optical study of Zeeman and Stark effects in crystalline benzophenone has been reported by Hochstrasser and Lin.[3]

The present report summarizes: general implications of the $n\pi^*$ triplet state in short-lived carbonyl hydrocarbons; an experimental technique that obviates the difficulty associated with the short lifetime of the $^3\Gamma_{n\pi^*}$ phosphorescent state in EMR study to the extent that the $\Delta M_s = \pm 2$ canonical field of benzophenone in ether glass at 77°K is observable; the extension of the application of the double-delta "1/2 electron" model previously reported[4-6] to the hypothetical pure $\pi\pi^*$ and $n\pi^*$ orbital excitation for benzophenone zero-field splitting (ZFS) as a function of the angular variation of the two-phenyl rings with respect to the plane containing the c = 0 groups; some inferences from experiments and computations and a discussion.

1. $n\pi^*$ Triplet in Carbonyl Hydrocarbons

The difficulty associated with the electron magnetic resonance (EMR) observation of the $^3\Gamma_{n\pi^*}$ state in some aromatic molecules containing a carbonyl group, >C = 0, is that the lifetime of the lowest triplet state is short ($\sim 10^{-3}$ sec), so that with the conventional method of irradiating the sample with a steady-state light source while sweeping the H field slowly (typically, $3 \sim 5 \times 10^3$ Oe/10 min), the steady-state concentration of $|T_1\rangle$ that is sufficient for EMR detection ($\sim 10^{13}$ spins) cannot be attained. The

*This work was supported by the Joint Services Electronics Programs (U.S. Army, U.S. Navy, and U.S. Air Force) under Contract DA 28-043-AMC-02536(E).

introduction of the carbonyl group(s) to the aromatic hydrocarbons causes a decrease in the phosphorescent lifetime, τ_p, the fluorescence quantum yield, Φ_F, and an increase in the phosphorescence quantum yield, Φ_p, the intersystem-crossing rate constant, k_{ISC}, and the oscillator strength, f, of the $|T_1\rangle \leftarrow |S_o\rangle$ transition. The variation in the intrinsic lifetime, τ_p^o, of the triplet state from molecule to molecule is determined by the variation of the spin-orbit matrix element according to the expression[7]

$$\left(\tau_p^o\right)^{-1} = \frac{64\pi^4\nu^3}{3hc^3} \sum_r \left| \frac{\langle S_p|\mathcal{H}'|T_1^r\rangle}{E_{S_p} - E_{T_1}} \right|^2 |\langle S_p|e\bar{r}|S_o\rangle|^2, \tag{1}$$

where ν is the Frank-Condon maximum of the $|T_1\rangle \rightarrow |S_o\rangle$ emission, $|T_1^r\rangle$ is the r^{th} magnetic component of the lowest triplet state $|T_1\rangle$, r indicates the values of $M_s = 0, \pm 1$, $|S_p\rangle$ is the so-called perturbing singlet state, and $|S_o\rangle$ is the lowest singlet or ground state.

The measured lifetime of phosphorescence, τ_p, cannot be totally determined by the matrix element (1), since it is a function of various quenching processes originating from the $|T_1\rangle$, as well as that of the rate of the emissive process (phosphorescence). τ_p can be written

$$\tau_p = \left[k_p + \sum k_{qi}\right]^{-1}, \tag{2}$$

where k_p is the rate constant for the phosphorescence, and k_{qi} represents various radiationless downward processes $|T_1\rangle \rightsquigarrow |S_o\rangle$. This means that the measured phosphorescence lifetime is subject to change with the molecular environment[8] and the impurities (for example, the bimolecular quenching of $|T_1\rangle$ of carbonyl hydrocarbons by the $X^3\Sigma_g^-$ state of oxygen).

The spin-orbit operator $\mathcal{H}'$ in (1) in the McClure central-field approach[9,10] assumes that the interaction is that for electrons in a spherically symmetric potential field, and if the "spin-other orbit coupling" term is assumed negligible it has the form

$$\mathcal{H}' = \sum_{i=1}^{n} A_i(\ell_{xi}s_{xi} + \ell_{yi}s_{yi} + \ell_{zi}s_{zi})$$

$$A_i \equiv \sum_{K=1}^{N} (r_{iK})^{-1} (\partial V(r_{iK})/\partial r_{iK})(2m^2c^2)^{-1}, \tag{3}$$

where ℓ_{xi} and s_{xi} are the operators for the x-component of orbital and spin angular

momenta of the i^{th} electron; i runs over electrons 1, 2, . . . , n and the K for the nuclei 1, 2, . . . , N; and r_{iK} is the separation between the i^{th} electron and the K^{th} nucleus. The shortening of τ_p^o upon the introduction of carbonyl oxygen(s) to the hydrocarbon may be rationalized by (3), an analog to the atomic heavy-atom effect. A more general form of $\mathcal{H}'$ in molecules has been proposed by Hameka.[11]

The effect of spin-orbit interaction in the ZFS parameters is treated by second-order perturbation theory by various workers.[12-14] No such calculation has been done, however, for the $|T_1\rangle \left({}^3\Gamma_{n\pi^*}\left({}^3A_2\right)\right)$ of benzophenone.

The molecular Hamiltonian that takes spin-orbit interaction into consideration is

$$\mathcal{H} = \mathcal{H}_o + \mathcal{H}_{ss} + \mathcal{H}_{so}.$$

The matrix elements H_{ij} now include the second-order term

$$H_{ij} = \langle {}^3\Psi_k^i | \mathcal{H}_{ss} | {}^3\Psi_k^j \rangle - \sum \frac{\langle {}^3\Psi_k^i | \mathcal{H}_{so} | {}^1\Psi_n \rangle \langle {}^1\Psi_n | \mathcal{H}_{so} | {}^3\Psi_k^j \rangle}{E_{{}^1\Psi_n} - E_{{}^3\Psi_k}}, \tag{5}$$

where ${}^3\Psi_k^i$ are the zero-order triplet wave functions with antisymmetric spatial part and three symmetric spin functions differing in $i = M_s = 0, \pm 1$. $\mathcal{H}_{so}$ in (5) may be taken as identical in form to $\mathcal{H}'$ in (1). The consequence of this treatment yields $\mathcal{H}_{so}$.

$$\mathcal{H}_{so} = [Z - 2^{-1}(X+Y)]S_z^2 + 2^{-1}(X-Y)\left(S_x^2 - S_y^2\right) - 2^{-1}Z\bar{S}^2, \tag{6}$$

where X, Y, and Z are principal values of $\mathcal{H}_{ss}$. Since

$$\bar{S}^2 = S_x^2 + S_y^2 + S_z^2, \tag{7}$$

we may combine (6) and (7) to yield the same form as (7):

$$\mathcal{H}_{spin} = \mathcal{H}_{ss} + \mathcal{H}_{so} = -\left(X'S_x^2 - Y'S_y^2 + Z'S_z^2\right). \tag{8}$$

This is equivalent to saying that the effect of the spin-orbit coupling on ZFS parameters can be computed from the theory, but is difficult to distinguish in an EMR experiment. The contribution of spin-orbit coupling to the ZFS parameter D (=3/2(X+Y)) of NH and CH_2 has been calculated by Fogel and Hameka,[12] and by McIver and Hameka,[10] and the values are $D_{so}(NH) = 0.268\ cm^{-1}$ and $D_{so}(CH_2) = 0.1128\ cm^{-1}$.

2. Experiment: Fast-Scan Flash-Synchronized EMR (F-F-EMR)

a. Instrument

The apparatus designed by K. W. Bowers[15] is the first of the modifications of X-band spectrometers to overcome the difficulties described by McGlynn and co-workers.[1] The

principal features that resulted in the successful observation of the $\Delta M_s = \pm 2$ transition of benzophenone and some of its derivatives are the following.

1. Capability of scanning approximately 250 Oe/25 msec.
2. Intense xenon flash ($2^{-1}CV^2 \sim 4500$ j) lifetime is stretched to 25 msec, and the triggering of the flash is synchronized to the scan of the magnetic field of the X-band spectrometer.
3. The spectrum for each scan is stored in a time-averaging computer, CAT, to allow the growth of the signal and the cancellation of the noise as the scan is repeated.

The extensive applicability and versatility of this apparatus in the study of excited state systems are illustrated as follows.

1. Study of polarized emission from the Zeeman-split multiplet levels.
2. Magnetophotoselection in short-lived triplet molecules.
3. Triplet → triplet or singlet → triplet energy transfer in glass.
4. Multiplet exciton migration in polymers and liquid crystals.
5. Study of short-lived intermediates in photospecific isomerization.

A block diagram of the fast-scanning flash-synchronized EMR spectrometer is shown in Fig. II-1. The capacitor bank (18,000 μF) is charged with a DC power supply to a maximum of 700 V, and discharged through the high-energy low-pressure xenon flash tube. The lifetime of the flash, that is, the 1/2 height of the flash contour (cf. Fig. II-2a) is adjusted to approximately 25 msec. The triggering of the flash is done by discharging the 1-μF (600 V) capacitor through the primary of the trigger transformer. The synchronization of the flash and the field scan (Fig. II-2b) is accomplished by a series of pulse and waveform generators, A, B, C, and F, the function generator, D, and the high-fidelity audio amplifier, E. A pulse of a few millivolts induced by the initial triggering is transformed by the waveform generator A into a sawtooth of ~40-msec duration; 20% of which triggers the pulse generator B in which the pulse height is amplified to ~15 V, and the pulsewidth ~1 msec. This amplified pulse fed into another waveform generator C gives a sawtooth of ~25-msec duration. The deviation of the slope from linearity is corrected by the function generator, D, and amplified by the 200-W audio-frequency amplifier to give a sawtooth of the amplitude necessary for the H field sweep. The monitoring of the shape and reproducibility of the flash, the input and the output of the audio amplifier is conveniently done by a multichannel vertical amplifier (Tektronix 3A74) and a 3B4 time base with a Type 576 storage oscilloscope.

For the accumulation of the signal from the excited paramagnetic sample (benzophenone, etc.), the conventional repeated-scan method is used. The synchronization of the time-averaging computer, CAT, which stores the spectrum is done similarly by having the pulse generator F give an ~3 V, 10^{-3} sec pulse to the CAT.

Since the H field scan is ~25 msec, the time constant of the factory-made 100-kHz modulation unit inside the Varian E-3 spectrometer is too large. A modification to the

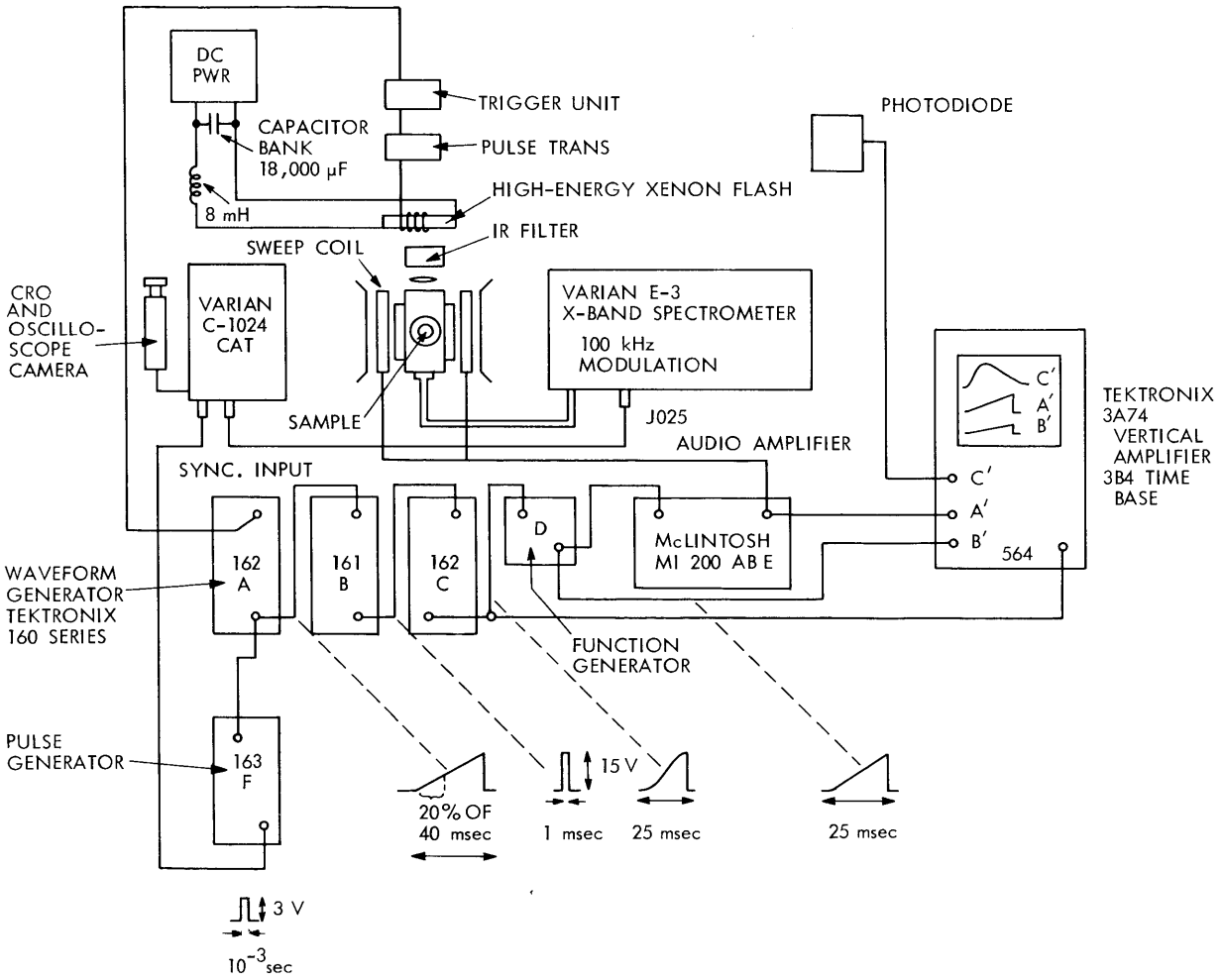

Fig. II-1. Fast-scan flash-synchronized X-band EMR spectrometer for short-lived excited states of molecules and atoms.

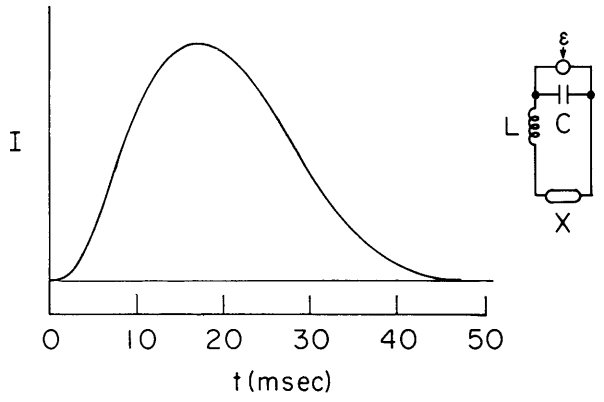

(a)

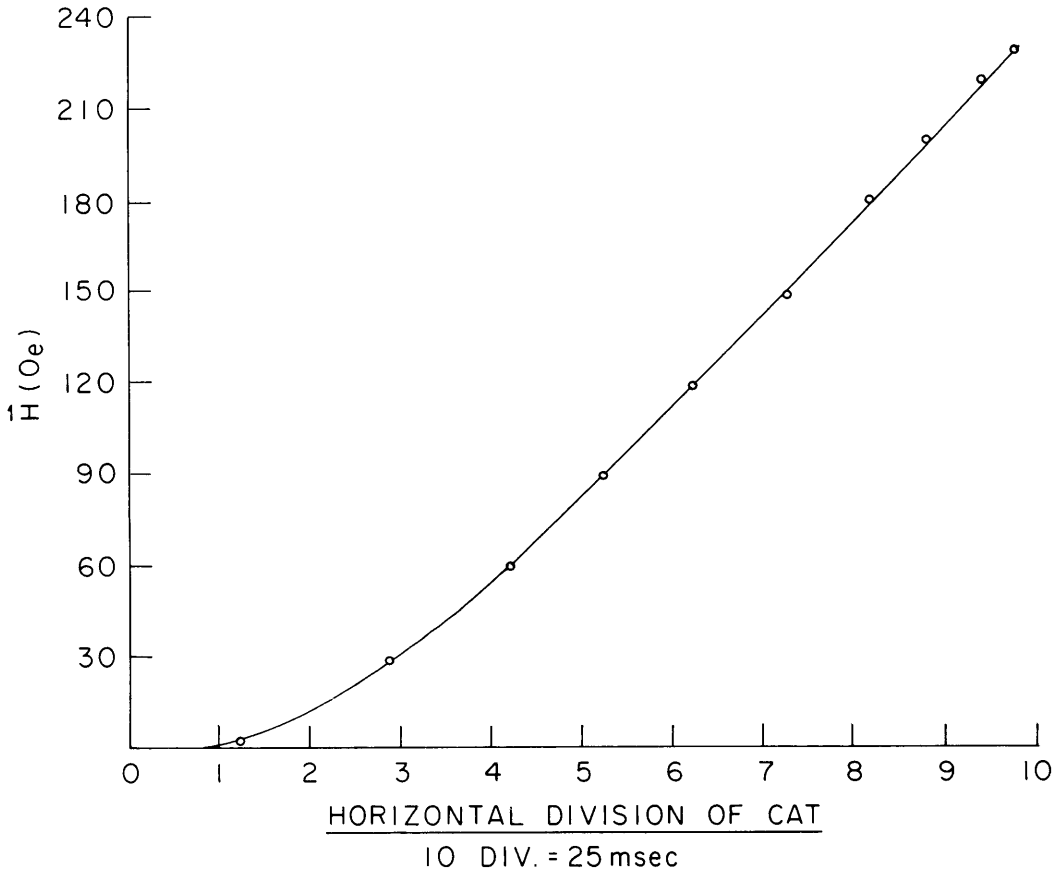

(b)

Fig. II-2. (a) Flash contour at C = 18,000 μF, E = 400 V, and L = 8 mH.
(b) Nearly linear relation of $\overline{H}$ field scan and the horizontal division of CAT.

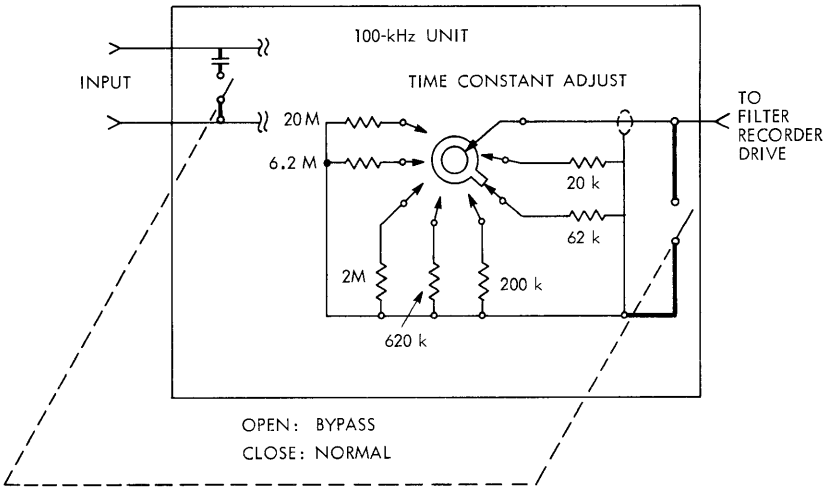

Fig. II-3. Heavy lines showing SPDT toggle switch added to 100-kHz unit of the E-3 spectrometer to be used for both normal scans and for F-F-EMR.

100-kHz unit is shown in Fig. II-3.

The $\Delta M_s = \pm 2$ fields of benzophenone, p-OH benzophenone, p-CH_3 benzophenone, p-NH_2 benzophenone, fluorene-9-one, benzyl, xanthane-9-one, and thio-xanthane-9-one are shown in Fig. II-4. The first four samples were recrystalized and sublimed several times, the last four came from the Beckman photosensitizer series without further purification.

The ether glass at 77°K and the quartz (Spectrosil) sample tube give a typical microwave resonance frequency, $\nu = 9.15 \pm$ GHz. The assignment of the observed signal as $\Delta M_s = \pm 2$ comes from the relative intensity of the $\Delta M_s = \pm 1$ and $\Delta M_s = \pm 2$ fields with that of the CH_3 radical signal.

A consistently reproducible "additional" field is observed for fluorene-9-one (see Fig. II-4c) at 2530 Oe and at 4580 Oe. These could well be two of the $\Delta M_s = \pm 1$ transitions. The concentration of samples are typically $\sim 10^{-1}$ M, dissolved in diethylether or EPA, degassed 5 ~ 6 times by the freeze-pump-thaw method and vacuum-sealed in quartz sample tubes of ~3 mm diameter. Then the sample is immersed in liquid nitrogen that is contained in a quartz dewar. Blank runs include: empty dewar, dewar with liquid nitrogen, dewar, liquid nitrogen, sample tube with solvent glass, and each of these blanks was tested for irradiation on and off. The quartz dewar at liquid N_2 temperature gave "impurity signals" at 3288, 3350, and 3400 Oe upon irradiation.

The instrument arrangement was usually: Field at t = 0, 1400 Oe; scan range ~210 Oe; time constant, "bypass" position; scan time 25 msec; modulation amplitude 5, 10, 20 Oe (depending on the width of the signal); receiver gain $1.25 \sim 5.0 \times 10^6$; temperature of the sample 77°K; microwave power 0.5 ~ 1.6 mW; microwave

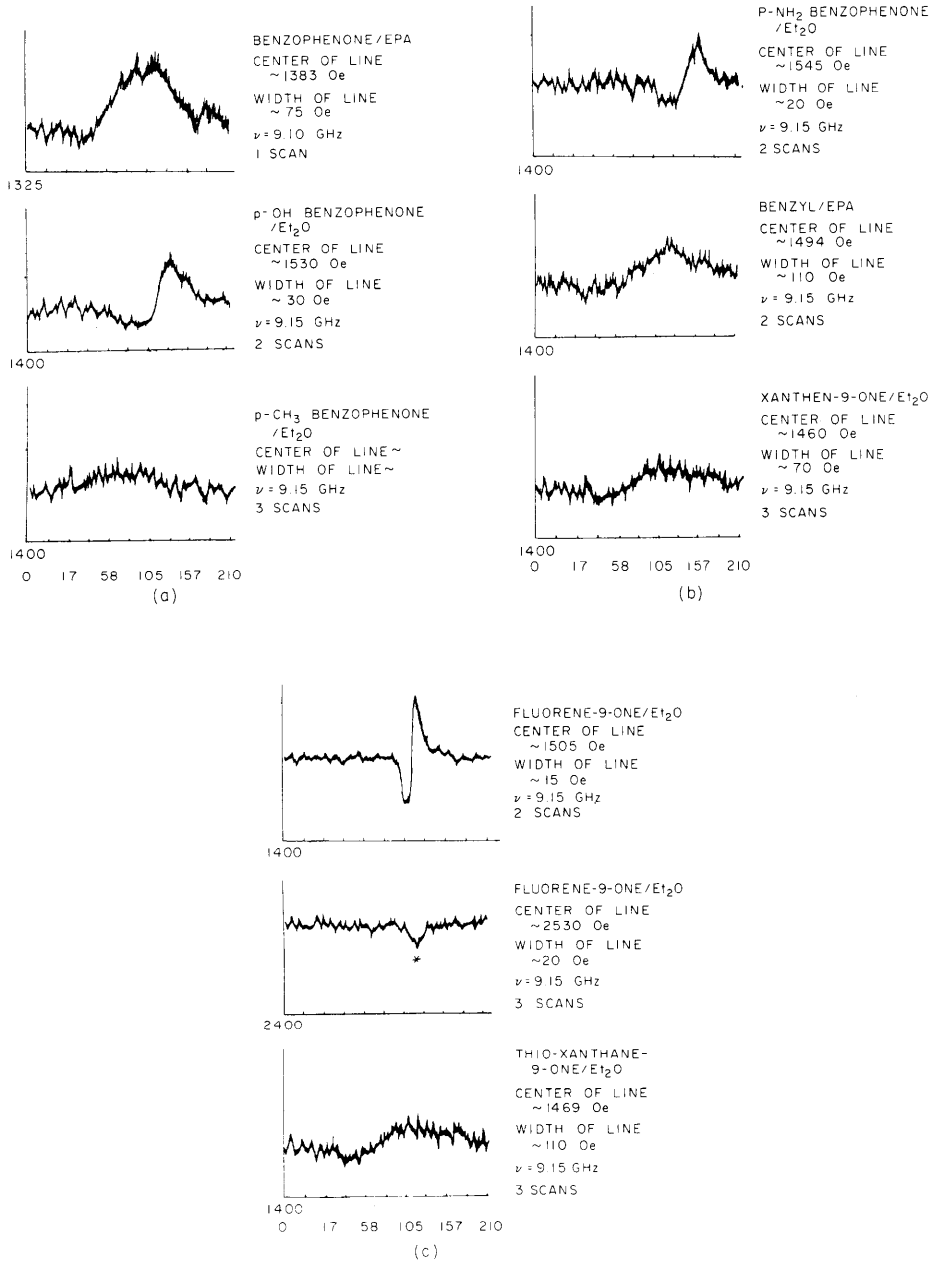

Fig. II-4. $\Delta M_s = \pm 2$ field of (a) benzophenone, p-OH benzophenone, and p-CH_3 benzophenone; (b) p-NH_2 benzophenone, benzyl, and xanthen-9-one; (c) fluorene-9-one, thio-xanthane-9-one, and "$\Delta M_s \pm 1$" of fluorene-9-one.

frequency 9.150 ± GHz. Noticeable are the linewidth and the shift of the $\Delta M_s = \pm 2$ fields.

Linewidth (for the numerical values in Oe see Fig. II-4).

p-CH_3 bzph > benzyl > bzph > xanthane-9-one
» p-OH bzph > p-NH_2 bzph > fluorene-9-one
(bzph = benzophenone)

Line position (for the numerical values in Oe see Fig. II-4).

bzph > xanthane-9-one > benzyl > fluorene-9-one
> p-OH bzph > p-NH_2 bzph.

The trends that have been observed will be discussed in section 4.

3. Double-delta "1/2-Electron" Model of Benzophenone: $\pi\pi^*$ and $n\pi^*$ Types

The derivation and the details of the model have been described in previous reports.[4-6] The molecule-fixed axes and carbon-atom labels are defined in Fig. II-5.

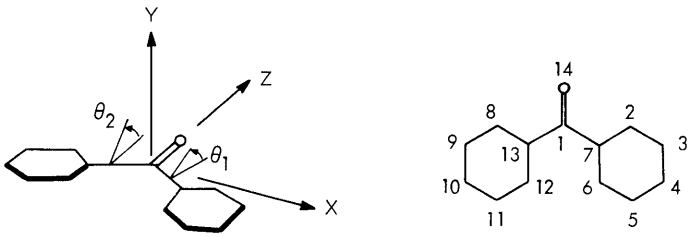

Fig. II-5. Axes, angles θ_1, θ_2, and labels for atoms.

For Hückel MO,

$$\beta_{ij} = \cos\theta_{ij}, \quad \text{for } i \neq j,\ i = 1,\ j = 13.$$

$$\beta_{ij} = -1, \quad \text{for } i = j, \tag{9}$$

$$\beta_{ij} = 0, \quad \text{for } i \neq j, \quad \text{if} \begin{cases} i \neq 1 \\ j \neq 7, 13 \end{cases}$$

The resonance parameter $k_{c=0} = \alpha_o + k\beta = -0.76$ (Wheland[16]), the Coulomb parameter $h_o = \chi_o - \chi_c = 1$ (Pauling[17]), and $k_{c-c}(1.45\ \text{Å}) = 0.91$ (Mulliken[18]) are used. The approximate zero-field splitting parameters, $\langle U(\theta_1, \theta_2)\rangle$, are calculated by using the double-delta "1/2-electron" model formula.

Table II-1(a). Eigenvectors and the components of the position vectors for benzophenone π, π^* triplet (a) and n, π^* triplet (b).

BENZOPHENONE (10,20) PI-PI* CONFIG

ATOM	XU	XL	YU	YL	ZU	ZL	CBOND	CABOND
1	0.0	0.0	-0.472	0.472	0.0	0.0	-0.095	0.534
2	1.684	1.766	-0.615	0.314	-0.082	0.060	0.186	-0.269
3	2.550	2.632	-0.615	0.314	-0.948	-0.806	-0.145	-0.055
4	2.557	2.639	-0.465	0.465	-1.937	-1.795	-0.319	0.290
5	1.698	1.780	-0.314	0.615	-2.060	-1.918	-0.145	-0.055
6	0.832	0.914	-0.314	0.615	-1.926	-1.784	0.186	-0.269
7	0.825	0.907	-0.465	0.465	-0.571	-0.429	0.315	0.156
8	-1.665	-1.747	-0.740	0.147	-0.185	0.095	0.178	-0.257
9	-2.531	-2.613	-0.740	0.147	-1.051	-0.771	-0.139	-0.052
10	-2.557	-2.639	-0.444	0.444	-2.006	-1.726	-0.304	0.276
11	-1.717	-1.799	-0.147	0.740	-2.095	-1.815	-0.139	-0.052
12	-0.851	-0.933	-0.147	0.740	-1.961	-1.681	0.178	-0.257
13	-0.825	-0.907	-0.444	0.444	-0.140	0.140	0.301	0.149
14	0.900	0.900	-0.472	0.472	0.900	0.900	-0.627	-0.469

ZFS-APPROXIMATION, DOUBLE DELTA FUNCTION

DAV, PROPORTIONAL TO D, IS 0.197E-01 EAV, PROPORTIONAL TO E, IS-0.258E 00

XAV # 0.264E 00 YAV #-0.251E 00 ZAV #-0.132E-01

CBOND = eigenvectors of the highest bonding MO.

CABOND = eigenvectors of the lowest antibonding MO.

XU = X component of the position vector for the delta function above phenyl plane.

XL = X component of the position vector for the delta function below phenyl plane.

$\theta_1 = 10°$.

$\theta_2 = 20°$.

$\{X_{AV}, Y_{AV}, Z_{AV}\} = \langle U(\theta) \rangle \propto$ ZFS.

Table II-1(b). Similar to Table II-1(a) except that various values are for hypothetical benzophenone pure n, π^* triplet having $\theta_1 = 10°$, $\theta_2 = 20°$.

BENZOPHENONE (10,20) N-PI* CONFIG

ATOM	XU	XL	YU	YL	ZU	ZL	CBOND	CABOND
1	0.0	0.0	-0.472	0.472	0.0	0.0	0.0	0.534
2	1.684	1.766	-0.615	0.314	-0.082	0.060	0.0	-0.269
3	2.550	2.632	-0.615	0.314	-0.948	-0.806	0.0	-0.055
4	2.557	2.639	-0.465	0.465	-1.937	-1.795	0.0	0.290
5	1.698	1.780	-0.314	0.615	-2.060	-1.918	0.0	-0.055
6	0.832	0.914	-0.314	0.615	-1.926	-1.784	0.0	-0.269
7	0.825	0.907	-0.465	0.465	-0.571	-0.429	0.0	0.156
8	-1.665	-1.747	-0.740	0.147	-0.185	0.095	0.0	-0.257
9	-2.531	-2.613	-0.740	0.147	-1.051	-0.771	0.0	-0.052
10	-2.557	-2.639	-0.444	0.444	-2.006	-1.726	0.0	0.276
11	-1.717	-1.799	-0.147	0.740	-2.095	-1.815	0.0	-0.052
12	-0.851	-0.933	-0.147	0.740	-1.961	-1.681	0.0	-0.257
13	-0.825	-0.907	-0.444	0.444	-0.140	0.140	0.0	0.149
14	0.900	0.900	-0.472	0.472	0.900	0.900	0.999	-0.469

ZFS-APPROXIMATION, DOUBLE DELTA FUNCTION

DAV, PROPORTIONAL TO D, IS-0.193E 00 EAV, PROPORTIONAL TO E, IS-0.137E 00

XAV # 0.724E-01 YAV #-0.201E 00 ZAV # 0.129E 00

Table II-2. Computed ZFS of benzophenone as functions of θ_1 and θ_2.

Orbital Promotion Type	θ_1 , θ_2	X_{av}	Y_{av}	Z_{av}	D_{av}	E_{av}
$\pi^* \leftarrow \pi$	0 , 0	.282	-.248	-.0341	.0511	-.265
$\pi^* \leftarrow n$	0 , 0	.0796	-.193	.114	-.171	-.136
$\pi^* \leftarrow \pi$	0 , 10	.276	-.260	-.0163	.0244	-.268
$\pi^* \leftarrow n$	0 , 10	.0734	-.200	.126	-.190	-.137
$\pi^* \leftarrow \pi$	0 , 20	.274	-.264	-.0100	.0151	-.269
$\pi^* \leftarrow n$	0 , 20	.0731	-.203	.130	-.195	-.138
$\pi^* \leftarrow \pi$	0 , 30	.269	-.271	.0015	-.0023	-.270
$\pi^* \leftarrow n$	0 , 30	.0726	-.209	.137	-.205	-.141
$\pi^* \leftarrow \pi$	0 , 45	.258	-.282	.0239	-.0359	-.270
$\pi^* \leftarrow n$	0 , 45	.0707	-.221	.151	-.226	-.146
$\pi^* \leftarrow \pi$	0 , 50	.254	-.287	.0327	-.0490	-.271
$\pi^* \leftarrow n$	0 , 50	.0696	-.227	.157	-.236	-.148
$\pi^* \leftarrow \pi$	0 , 60	.251	-.300	.0487	-.0730	-.276
$\pi^* \leftarrow n$	0 , 60	.0663	-.236	.170	-.255	-.151
$\pi^* \leftarrow \pi$	0 , 70	.258	-.319	.0612	-.0918	-.288
$\pi^* \leftarrow n$	0 , 70	.0631	-.246	.183	-.274	-.154
$\pi^* \leftarrow n$	0 , 80	.0604	-.253	.192	-.288	-.156
$\pi^* \leftarrow \pi$	0 , 85	.268	-.340	.0718	-.108	-.304
$\pi^* \leftarrow n$	0 , 85	.0594	-.254	.195	-.293	-.157
$\pi^* \leftarrow \pi$	10 , 10	.275	-.254	-.0207	.0310	-.264
$\pi^* \leftarrow n$	10 , 10	.0727	-.198	.125	-.187	-.135
$\pi^* \leftarrow \pi$	10 , 20	.264	-.251	-.0132	.0197	-.258
$\pi^* \leftarrow n$	10 , 20	.0724	-.201	.129	-.193	-.137
$\pi^* \leftarrow \pi$	10 , 30	.253	-.251	-.0018	.0028	-.252
$\pi^* \leftarrow n$	10 , 30	.0718	-.207	.135	-.203	-.139
$\pi^* \leftarrow \pi$	10 , 45	.240	-.259	.0194	-.0291	-.250
$\pi^* \leftarrow n$	10 , 45	.0692	-.219	.150	-.224	-.144
$\pi^* \leftarrow \pi$	10 , 50	.239	-.266	.0269	-.0403	-.253
$\pi^* \leftarrow \pi$	10 , 60	.242	-.283	.0417	-.0625	-.263
$\pi^* \leftarrow n$	10 , 60	.0651	-.234	.169	-.254	-.150
$\pi^* \leftarrow \pi$	10 , 70	.250	-.305	.0550	-.0825	-.277
$\pi^* \leftarrow n$	10 , 70	.0618	-.244	.182	-.273	-.153
$\pi^* \leftarrow \pi$	10 , 80	.259	-.325	.0652	-.0979	-.292
$\pi^* \leftarrow n$	10 , 80	.0587	-.250	.192	-.288	-.155
$\pi^* \leftarrow \pi$	10 , 85	.263	-.331	.0681	-.102	-.297
$\pi^* \leftarrow n$	10 , 85	.0579	-.252	.195	-.292	-.155
$\pi^* \leftarrow \pi$	20 , 20	.271	-.245	-.0257	.0385	-.258

Table II-2. (continued)

Orbital Promotion Type	θ_1 , θ_2	X_{av}	Y_{av}	Z_{av}	D_{av}	E_{av}
$\pi^* \leftarrow n$	20 , 20	.0717	-.198	.126	-.189	-.135
$\pi^* \leftarrow \pi$	20 , 45	.237	-.246	.0088	-.0132	-.241
$\pi^* \leftarrow n$	20 , 45	.0680	-.216	.148	-.222	-.142
$\pi^* \leftarrow \pi$	20 , 50	.232	-.250	.0175	-.0262	-.241
$\pi^* \leftarrow n$	20 , 50	.0682	-.220	.152	-.228	-.144
$\pi^* \leftarrow \pi$	20 , 60	.233	-.265	.0317	-.0476	-.249
$\pi^* \leftarrow n$	20 , 60	.0637	-.232	.168	-.252	-.148
$\pi^* \leftarrow \pi$	20 , 70	.238	-.284	.0456	-.0684	-.261
$\pi^* \leftarrow n$	20 , 70	.0598	-.241	.181	-.272	-.150
$\pi^* \leftarrow \pi$	20 , 80	.246	-.302	.0559	-.0838	-.274
$\pi^* \leftarrow n$	20 , 80	.0564	-.248	.192	-.288	-.152
$\pi^* \leftarrow \pi$	20 , 85	.249	-.308	.0587	-.0881	-.278
$\pi^* \leftarrow n$	20 , 85	.0557	-.251	.195	-.292	-.153
$\pi^* \leftarrow \pi$	30 , 30	.265	-.234	-.0315	-.0472	-.250
$\pi^* \leftarrow n$	30 , 30	.0716	-.202	.130	-.195	-.137
$\pi^* \leftarrow \pi$	30 , 45	.226	-.229	.0026	-.0038	-.228
$\pi^* \leftarrow n$	30 , 45	.0687	-.214	.146	-.218	-.141
$\pi^* \leftarrow \pi$	30 , 50	.231	-.233	.0018	-.0027	-.232
$\pi^* \leftarrow n$	30 , 50	.0671	-.220	.153	-.229	-.143
$\pi^* \leftarrow \pi$	30 , 60	.223	-.241	.0180	-.027	-.232
$\pi^* \leftarrow n$	30 , 60	.0634	-.231	.167	-.251	-.147
$\pi^* \leftarrow \pi$	30 , 70	.224	-.256	.0326	-.0488	-.240
$\pi^* \leftarrow n$	30 , 70	.0590	-.242	.183	-.274	-.150
$\pi^* \leftarrow \pi$	30 , 80	.227	-.217	.0441	-.0661	-.249
$\pi^* \leftarrow \pi$	30 , 85	.229	-.276	.0473	-.0710	-.252
$\pi^* \leftarrow n$	30 , 85	.0543	-.252	.198	-.296	-.153
$\pi^* \leftarrow \pi$	45 , 45	.255	-.216	-.0392	.0587	-.235
$\pi^* \leftarrow n$	45 , 45	.0739	-.216	.142	-.213	-.145
$\pi^* \leftarrow \pi$	45 , 50	.240	-.212	-.0280	.0419	-.226
$\pi^* \leftarrow n$	45 , 50	.0724	-.222	.150	-.225	-.147
$\pi^* \leftarrow \pi$	45 , 60	.217	-.209	-.0080	.0119	-.213
$\pi^* \leftarrow n$	45 , 60	.0683	-.235	.167	-.250	-.152
$\pi^* \leftarrow \pi$	45 , 70	.202	-.214	.0117	-.0175	-.208
$\pi^* \leftarrow n$	45 , 70	.0634	-.248	.185	-.277	-.156
$\pi^* \leftarrow \pi$	45 , 80	.194	-.222	.0280	-.0419	-.208
$\pi^* \leftarrow n$	45 , 80	.0583	-.259	.201	-.301	-.159
$\pi^* \leftarrow \pi$	45 , 85	.192	-.225	.0332	-.0498	-.209

Table II-2. (concluded)

Orbital Promotion Type	θ_1 , θ_2	X_{av}	Y_{av}	Z_{av}	D_{av}	E_{av}
$\pi^* \leftarrow n$	45 , 85	.0568	-.261	.205	-.307	-.159
$\pi^* \leftarrow \pi$	50 , 50	.251	-.209	-.0419	.0629	-.230
$\pi^* \leftarrow n$	50 , 50	.0763	-.223	.147	-.220	-.150
$\pi^* \leftarrow \pi$	50 , 60	.221	-.202	-.0192	.0288	-.211
$\pi^* \leftarrow n$	50 , 60	.0724	-.237	.165	-.247	-.155
$\pi^* \leftarrow \pi$	50 , 70	.198	-.202	.0035	-.0052	-.200
$\pi^* \leftarrow n$	50 , 70	.0671	-.252	.185	-.277	-.159
$\pi^* \leftarrow \pi$	50 , 80	.184	-.208	.0237	-.0355	-.196
$\pi^* \leftarrow n$	50 , 80	.0618	-.263	.201	-.302	-.163
$\pi^* \leftarrow \pi$	50 , 85	.180	-.211	.0306	-.0459	-.195
$\pi^* \leftarrow n$	50 , 85	.0602	-.267	.206	-.310	-.163
$\pi^* \leftarrow \pi$	60 , 60	.243	-.195	-.0485	.0727	-.219
$\pi^* \leftarrow n$	60 , 60	.0845	-.240	.155	-.233	-.162
$\pi^* \leftarrow \pi$	60 , 70	.124	-.131	.0078	-.0117	-.128
$\pi^* \leftarrow n$	60 , 70	.0799	-.257	.177	-.266	-.169
$\pi^* \leftarrow \pi$	60 , 80	.169	-.187	.0185	-.0277	-.178
$\pi^* \leftarrow n$	60 , 80	.0742	-.272	.198	-.297	-.173
$\pi^* \leftarrow \pi$	60 , 85	.157	-.189	.0317	-.0475	-.173
$\pi^* \leftarrow n$	60 , 85	.0725	-.276	.204	-.306	-.174
$\pi^* \leftarrow \pi$	70 , 70	.238	-.185	-.0536	.0804	-.212
$\pi^* \leftarrow n$	70 , 70	.102	-.263	.161	-.242	-.183
$\pi^* \leftarrow \pi$	70 , 80	.175	-.186	.0105	-.0157	-.181
$\pi^* \leftarrow n$	70 , 80	.0996	-.283	.183	-.275	-.191
$\pi^* \leftarrow \pi$	70 , 85	.146	-.189	.0430	-.0645	-.167
$\pi^* \leftarrow n$	70 , 85	.0983	-.289	.191	-.286	-.194
$\pi^* \leftarrow \pi$	80 , 80	.244	-.193	-.0513	.0770	-.219
$\pi^* \leftarrow n$	80 , 80	.134	-.295	.161	-.242	-.215
$\pi^* \leftarrow \pi$	80 , 85	.174	-.208	.0346	-.0519	-.191
$\pi^* \leftarrow n$	80 , 85	.135	-.305	.169	-.254	-.220
$\pi^* \leftarrow \pi$	85 , 85	.381	-.176	-.205	.308	-.279
$\pi^* \leftarrow n$	85 , 85	.157	-.313	.156	-.233	-.235

$$\langle U(\theta_1, \theta_2)\rangle = \sum_i \sum_k C_i(\theta_1, \theta_2)\, C_k(\theta_1, \theta_2) \{C_i(\theta_1, \theta_2)\, C_k(\theta_1, \theta_2) - C_k(\theta_1, \theta_2)\, C_i(\theta_1, \theta_2)\} \left[\{\mathscr{U}(\theta_1, \theta_2)\}_{i_1^+ k_2^+} + \{\mathscr{U}(\theta_1, \theta_2)\}_{i_1^+ k_2^-} + \{\mathscr{U}(\theta_1, \theta_2)\}_{i_1^- k_2^+} + \{\mathscr{U}(\theta_1, \theta_2)\}_{i_1^- k_2^-} \right], \tag{10}$$

where $U \equiv X, Y, Z$, $\mathscr{U} \equiv \mathscr{X}, \mathscr{Y}, \mathscr{Z}$ (for the definition of each operator see previous reports[4-6]), $C_n(\theta_1, \theta_2)$ are Hückel AO coefficients at atomic position n, $\{\mathscr{U}(\theta_1, \theta_2)\}_{i_1^+ k_2^-}$ refers to the ZFS operators $\mathscr{X}$, $\mathscr{Y}$, and $\mathscr{Z}$ evaluated with electron 1 at the nucleus i above the phenyl-ring plane, and electron 2 at the nucleus k below the phenyl-ring plane.

Furthermore, two orbital excitation types $\pi\pi^*$ and $n\pi^*$ are assumed to involve only the promotion of an electron of n or of the highest π bonding orbital into the lowest antibonding π^* orbital. Typical position vectors for the delta functions at various nuclear positions above and below the phenyl-ring plane are shown in Table II-1. The results of the computation of Eq. 10 for both pure $\pi\pi^*$ and $n\pi^*$ triplet states of benzophenone are

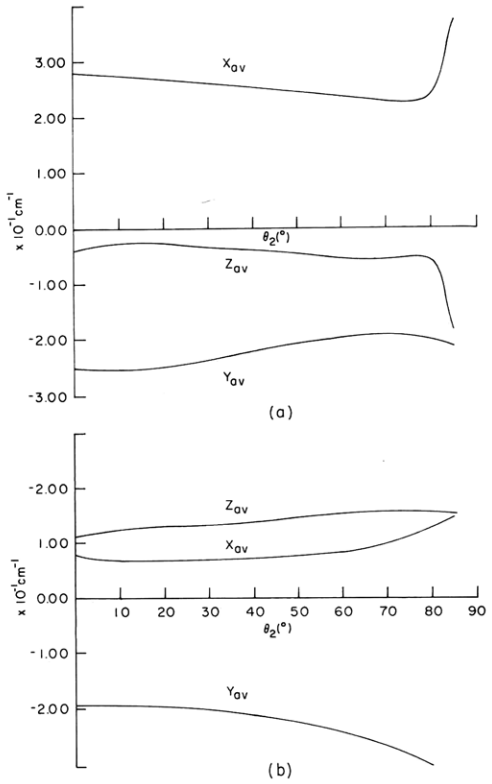

Fig. II-6. (a) $\langle U(\theta)\rangle$ for benzophenone $\pi^* \leftarrow \pi$ triplet $\theta_1 = \theta_2$.
(b) $\langle U(\theta)\rangle$ for benzophenone $\pi^* \leftarrow$ n triplet $\theta_1 = \theta_2$.

listed in Table II-2. Figure II-6 shows the behavior of the approximate expectation of ZFS, that is, $\langle U(\theta_1, \theta_2)\rangle = X_{av}, Y_{av}, Z_{av}$ in the case of $\theta_1 = \theta_2$ for $\pi\pi^*$ and $n\pi^*$ triplet

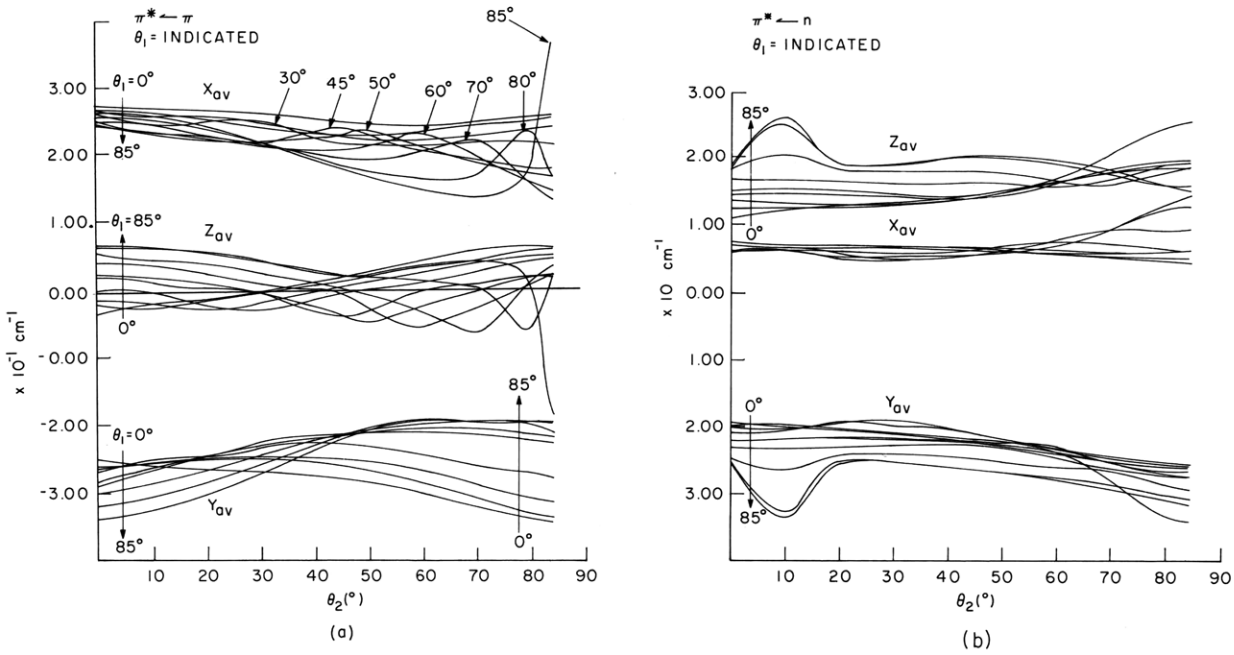

Fig. II-7. Computed principal values of the dipolar tensor of benzophenone (a) under the assumption of pure $\pi^* \leftarrow \pi$ triplet $\theta_1 = \theta_2$ and $\theta_1 \neq \theta_2$; (b) under the assumption of pure $\pi^* \leftarrow n$ triplet $\theta_1 = \theta_2$ and $\theta_1 \neq \theta_2$.

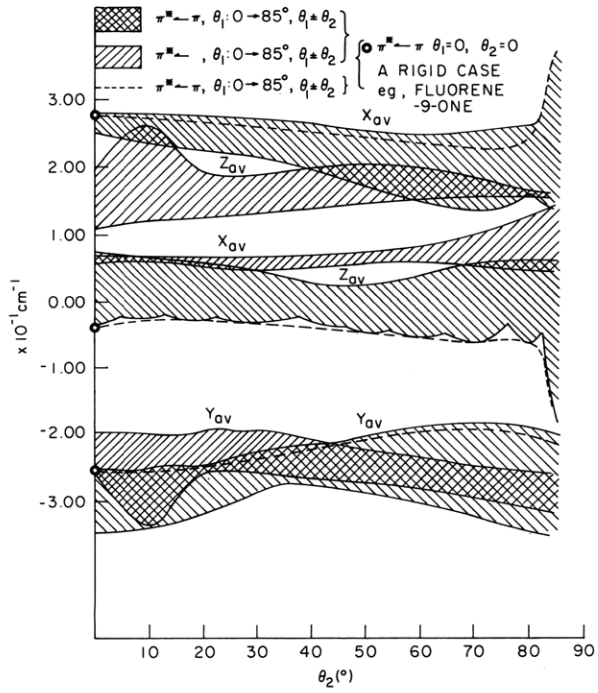

Fig. II-8. Uncertainty of principal values with assumed free rotation of phenyl rings.

states, respectively. Figure II-7 exhibits the superposition of $\langle U(\theta_1, \theta_2)\rangle$ for several possible combinations of θ_1 and θ_2. Figure II-8 shows a comparison of the uncertainty of the principal values $\Delta\langle U(\theta_1, \theta_2)\rangle$ of the $\pi\pi^*$ triplet and that of the $n\pi^*$ triplet and points out that if θ_1 and θ_2 are equal and fixed (such as in the case of fluorene-9-one), we should expect a sharp resonance line.

4. Conclusions and Discussion

We may now inquire, "What do the observed and the computed results mean?" The most obvious observed trends are those of linewidth and line position.

(a) Linewidth

The linewidth $\lambda_{k\ell}$ for the $|k\rangle \rightarrow |\ell\rangle$ transition can be approximated by[19]

$$\lambda_{k\ell} = 2h\left|\partial H/\partial\delta\right|\left[\langle \Delta\nu^2\rangle_{k\ell}\right]^{1/2}, \tag{11}$$

where $\langle \Delta\nu^2\rangle_{k\ell}$ is the second moment arising from the nuclear Zeeman and the electron-nucleus couplings, and $\partial H/\partial\delta$, $\delta = h\nu_{\text{microwave}}$ is the field-shift operator. The former can be expressed as

$$\langle \Delta\nu^2\rangle = 4^{-1}\left\{\sum_N \left(h^{-1}g_N\beta_\rho\right)^2 \left|\bar{H}_{kN}-\bar{H}_{\ell N}\right|^2 + \sum_{N'} \left|\langle k|S|k\rangle - \langle \ell|\bar{S}|\ell\rangle\right|^2\right\} \tag{12}$$

and

$$\bar{H}_{kN} = h(g_N\beta_\rho)^{-1}\,\langle k|\bar{\bar{T}}_N \cdot \bar{S}|k\rangle,$$

where g_N is the nuclear g factor, $\beta_\rho = eh/2Mc$ is the nuclear magneton, $\bar{\bar{T}}$ is the hyperfine interaction tensor, $\bar{S}$ is the total electron spin operator, and $\partial H/\partial\delta$ in the $\delta = h\nu_{\text{const.}}$ experiment has the following form[20]:

$$\frac{\partial H}{\partial\delta} = \delta H\left[3\delta^2+9v-9(g\beta H)^2\right] \times \left[2(\delta^2+v)\left\{4v+\delta^2-2(g\beta H)^2\right\}\right.$$

$$\left. + 4(g\beta H)^2 \pm 6\sqrt{3}\,XYZ\left\{4(g\beta H)^2-\delta^2-4v\right\}^{1/2}\right]^{-1} \tag{13}$$

$$v = XY + YZ + ZX.$$

Equations 11-13 imply that for an assembly of randomly oriented molecules the major contributions to the linewidth come from (i) the nucleon-electron interaction, (ii) the electron spin-spin interaction, and (iii) the deviation of the ZFS parameter, because of the molecular motion (vibration, internal rotation, etc.). In view of these considerations,

the significant linewidth gap between benzophenone and fluorene-9-one becomes quite reasonable (see Fig. II-9).

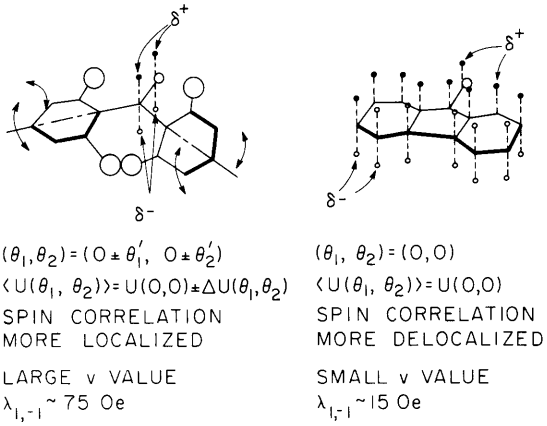

Fig. II-9. Comparative inferences about ZFS of benzophenone and the fluorene-9-one triplet.

During the flash excitation, 25×10^{-3} sec, the $|T_1^r\rangle$ electronic states are populated. For the benzophenone the "snapshot" of the transitions between the r = +1 and r = -1 magnetic components is blurred, because of the greater value of v and the deviation (uncertainty) in $\langle U(\theta_1,\theta_2)\rangle$, while the "picture" of the fluorene-9-one is clear-cut, except for the finite width arising from $\langle \Delta\nu^2\rangle$.

(b) Line Position of $\Delta M_s = \pm 2$

The theoretical line position of $\Delta M_s = \pm 2$ has at most four components. These arise from the canonical orientations and the stationary resonance condition. They are

$$H_{min} = (2g\beta)^{-1}[\delta^2+4v]^{1/2}$$
$$H'_x = (2g\beta)^{-1}[\delta^2-(Y-X)]^{1/2}. \qquad (14)$$

H'_y and H'_z follow the permuting order of XYZ, and if H_{min} exists for a given $\delta = h\nu_{microwave}$, it dominates the rest and H'_x, H'_y, and H'_z are likely to become little shoulders of H_{min}. In any case, from (11)-(14) it can readily be seen that both linewidth and line position are dependent on the values and deviations of $\langle U(\theta_1,\theta_2)\rangle$.

The results of the computation (Figs. II-6 through II-8) suggest that the deviation of $\langle U(\theta_1,\theta_2)\rangle$ is appreciable and causes significant line broadening, provided that in $|T_1\rangle$ θ_1 and θ_2 of benzophenone vary, because of the degree of freedom within the limit determined by various nonbonded interactions.

We may generalize that the spin-spin interaction in a molecule possessing greater degree of vibrational or internal rotational freedom tends to increase, and the

uncertainty of its expectation increases. In a molecule possessing less degree of motional freedom the spin-spin correlation tends to decrease, and the uncertainty of its expectation decreases. Benzophenone and fluorene-9-one typify this generalization, and the alteration imposed by introducing substituent(s) upon the dipolar spin correlation should also follow this simple inference. The observed order of linewidth and line position are consistent with these conclusions.

Despite the great advantage of the apparatus, the only "possible $\Delta M_s = \pm 1$" observed among short-lived $n\pi^*$ triplets is that of fluorene-9-one. No detailed structure of the phosphorescent state can be deduced from $\Delta M_s = \pm 2$ alone for the sample in a glass (because of its near isotropy).

The search for the $\Delta M_s = \pm 1$ transition by line symmetry is unreliable, since the resonance condition is dependent upon the principal values. For example, for a sample having $D = 1.00$ and $|E| = 0.002$, there is only one EMR line ($\Delta M_s = \pm 2$, not H_{min}) within $1400 < H \leq 4999$ Oe. For $D = 0.500$, $|E| = 0.002$ there are no $\Delta M_s = \pm 2$; only two $\Delta M_s = \pm 1$ fields appear. For $D \geq 2.00$, $|E| = 0.002$ no EMR field can be found in the X-band observation.

Although no consideration of intermolecular forces was attempted in this work, the migration of excitation (exciton) in fairly concentrated rigid glass cannot be ignored. The formation of excited dimer and various anomalies encountered in EMR work when the intermolecular distance is small will be examined in the future. Various models of excitonic phenomena may be employed in such studies.[21-23]

The authors would like to thank Professor D. M. Hercules and A. Vaudo for their assistance.

K. W. Bowers, B. S. Yamanashi, C. Mazza

References

1. S. P. McGlynn, T. Azumi, and M. Kinoshita, Molecular Spectroscopy of the Triplet State (Prentice-Hall Inc., Englewood Cliffs, N.J., 1968), pp. 166-172.
2. C. Thomson, Quart. Revs. Quantum Phys. 22, 45 (1968).
3. R. M. Hochstrasser and T-S Lin, J. Chem. Phys. 49, 4929 (1968).
4. K. W. Bowers, Quarterly Progress Report No. 89, Research Laboratory of Electronics, M.I.T., April 15, 1968, pp. 7-18.
5. B. S. Yamanashi, Quarterly Progress Report No. 91, Research Laboratory of Electronics, M.I.T., October 15, 1968, pp. 61-72.
6. B. S. Yamanashi and K. W. Bowers, Quarterly Progress Report No. 92, Research Laboratory of Electronics, M.I.T., January 15, 1969, pp. 43-59.
7. S. P. McGlynn, T. Azumi, and M. Kinoshita, op. cit., p. 263.
8. E. L. Wehry, in Fluorescence, G. G. Gilbault (ed.) (Mercel Dekker, Inc., New York, 1967).
9. D. S. McClure, J. Chem. Phys. 17, 665 (1949); 23, 1772 (1955).
10. D. S. McClure, J. Chem. Phys. 20, 682 (1952).

11. H. F. Hameka, in The Triplet State, A. B. Zahlan (ed.) (Cambridge University Press, London, 1967), pp. 1-27.

12. S. J. Fogel and H. F. Hameka, J. Chem. Phys. 42, 132 (1965).

13. J. W. McIver and H. F. Hameka, J. Chem. Phys. 45, 767 (1966); 46, 825 (1967).

14. J. B. Lounsbury, J. Chem. Phys. 42, 1549 (1965); 46, 2193 (1967).

15. K. W. Bowers and C. Mazza, Bull. Am. Phys. Soc. 13, 170 (1968).

16. G. W. Wheland, J. Am. Chem. Soc. 64, 900 (1942).

17. L. Pauling, The Nature of the Chemical Bond (Cornell University Press, Ithaca, N. Y., 2d edition, 1940), p. 134.

18. R. S. Mulliken, C. A. Rice, and D. Orloff, J. Chem. Phys. 17, 1248 (1949).

19. A. Abragam, The Principles of Nuclear Magnetism (Clarendon Press, Oxford, 1961), pp. 103-132.

20. P. Kottis and R. Lefebre, J. Chem. Phys. 41, 379 (1964).

21. A. S. Davydov, Theory of Molecular Exciton (McGraw-Hill Book Company, New York, 1961).

22. D. P. Craig and S. H. Walmsleg, Exciton in Molecular Crystals (Benjamin, New York, 1968).

23. S. I. Choi, I. Jortner, S. A. Rice, and R. Silbey, J. Chem. Phys. 41, 3294 (1964).